Fault Modeling for GBAS Airworthiness Assessments

Tim Murphy, Matt Harris– *Boeing*
Curt Shively – *Mitre*
Laurent Azoulai – *Airbus*
Mats Brenner – *Honeywell*

BIOGRAPHY

Tim Murphy is a Technical Fellow with Boeing Commercial Airplanes where he is a member of the Electronic Systems organization. Tim has 27 years of experience in radio navigation communications and surveillance systems for civil aviation. The current focus of his work is avionics for new airplane product development, and next generation CNS technologies to support Air Traffic Management including satellite navigation. Tim is very active in the development of international standards for use of satellite navigation by commercial aviation. He received a BSEE and MSEE from Ohio University.

Matt Harris is a Systems Engineer at The Boeing Company. He is involved in various aspects of communication, navigation, and surveillance research as a member of the Air Traffic Management Group within Boeing Commercial Airplanes. Matt has been very active in the development of the latest international GBAS standards at ICAO and RTCA. Matt received his Bachelor of Science and Master of Science in Electrical Engineering from Ohio University.

Curt Shively is a member of the Principal Staff at MITRE/CAASD. He has studied the use of satellites for communications, navigation and surveillance. He received his B.S. and M.S. in Electrical Engineering from the Massachusetts Institute of Technology..…

Laurent Azoulai is GNSS-Landing Systems Technical Expert with Airbus Operations, where he belongs to Navigation Department. His activities focus on future Approach and Landing architectures and the foreseen extended use of GNSS in Communication, Navigation and Surveillance aircraft systems. He is involved in standardization activities dealing with GBAS Cat 2/3, GPS/Galileo combination and SBAS for which he is co-chairman of RTCA SC-159 SBAS Working Group. He graduated in 1996 from Institut Supérieur de l'Electonique de Paris as an engineer specialized in automatic systems and pursued his whole career in the Navigation domain.

Mats Brenner is a senior engineering fellow at Honeywell guidance and navigation center of excellence. He graduated from the Royal Institute of Technology in Stockholm Sweden in 1974 with a degree in Engineering Physics and Mathematics. Mats has been developing algorithms and system architectures for GPS since 1984.

ABSTRACT

A new type of service has been proposed for Ground Based Augmentation System (GBAS) that is intended to support approach and landing operations down to the lowest minimums (i.e. CAT IIIb). Proposed standards for this new service type have been drafted and are currently being validated. This so called GBAS Approach Service Type D (GAST D) includes new low level requirements for monitoring as well as a requirement for additional geometry screening in order to protect the user from failures of several types. This paper discusses how the proposed requirements can be interpreted in order to develop a fault model that describes the magnitude and dynamics of malfunction induced navigation systems errors that are undetected or prior to detection. Such a fault model can be used to demonstrate acceptable airplane system level responses to malfunctions as part of airworthiness approvals. The paper includes a review of the types of malfunctions that are anticipated and the monitoring requirements that limit the impact of those malfunctions. Then a dynamic error model is proposed and the parameters of that model are presented for each type of failure. The relationship between the largest undetected errors and the user defined geometry screening is explored for each type of malfunction. Some discussion of how this model is anticipated to be used in the context of airworthiness demonstrations is included. This work represents an important step towards development of airworthiness requirements needed in order for GBAS to support CAT III operations in the future.

INTRODUCTION

The International Civil Aviation Organization (ICAO) Navigation System Panel (NSP) has been developing standards for GBAS since 1993. The initial Standards and Recommended Practices (SARPs) for GBAS were finished in the year 2000 and defined a system that was intended to support approach operations to CAT I minimums. Since that time, significant work has been done to extend these SARPs to enable GBAS to support operations to the lowest minimums (i.e. CAT IIIb). [1, 2, 3, 4, 5, 6, 7] This effort recently reached a milestone with the development and technical validation of SARPs which introduce a new type of GBAS service that is intended to support all categories of landing operations.

Airworthiness approval of airplanes with precision approach capabilities requires a significant safety analysis which includes analysis and simulation of aircraft performance under normal, limit and faulted conditions. [8, 9] Airplanes with automatic landing capabilities must be shown to have adequate performance. This demonstration is achieved through a combination of a statistical approach using Monte-Carlo autoland simulations, and a deterministic approach using simulator sessions with pilot in the loop and flight tests. Such simulations require a noise model to simulate representative errors and test their effects on performance of the landing system. Work on a suitable GBAS Noise Model has been underway since 1996 [10].

A GBAS noise model has been developed including extensions to the model to cover GAST D nominal noise expectations, limit case errors and simulation of limit conditions and fault modes [11]. The history of the development of the noise model is outlined in a previous paper [12]. The development of this model can be attributed to the efforts of many individuals over several years and the model continues to evolve as the GBAS standards have evolved to include GAST D [13, 14, 15, 16, 17, 18, 19, 20, 21, 22, 23, 24]. The most up-to-date proposal for the GBAS Landing System (GLS) noise model is given in Attachment A of reference [11]. It is expected that the model will continue to be refined by Boeing, Airbus and other interested parties and will ultimately be documented in updates to state airworthiness approval criteria (e.g. references [8] and [9]). Reference [11] shows that the proposed GAST D SARPS and DO-253C MOPS provide requirements that are complete enough so that a signal model supporting airworthiness assessments can be derived.

This paper specifically focuses on the derivation of the fault model included in the GBAS noise model. The intent of the fault model is to simulate the behavior of the GBAS at the output of the airborne GBAS equipment given a failure in some element of the GBAS system (i.e. the ground subsystem or the space segment). The fault model is based on the assumption that the GBAS ground station and airborne equipment correctly perform their intended function and that faults will eventually be detected and mitigated by the system. The fault model describes the behavior of the system after the fault has occurred and until the fault is detected and mitigated.

ANTICIPATED AIRWORTHINESS ASSESSMENT REQUIREMENTS FOR GLS TO SUPPORT CAT III OPERATIONS

The current airworthiness criteria are found in FAA Advisory Circular AC 120-28D [8] and EASA CS AWO Subpart 1 [9]. Requirements within these documents can be used as a model to define success criteria for total system landing performance. These requirements and the associated success criteria are discussed below.

There are 3 key conditions for which airworthiness requirements exist regarding performance. These 3 conditions are: system performance under nominal conditions, performance in a limit case condition and performance in the presence of malfunction. For each of these conditions defined in [8] and [9] acceptable performance is based on successfully landing inside a certain region of the runway (or not landing outside the limits of that region). The landing box is illustrated in Figure 1. Table 1 summarizes the three conditions and associated existing airworthiness requirements. The table also briefly outlines or paraphrases the success criteria for the existing requirements that may be used to establish equivalent safety performance has been achieved at the system level.

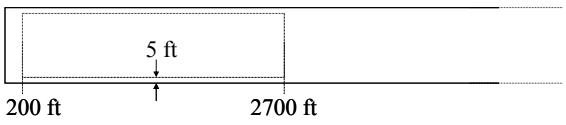

Figure 1 Landing Box Used to Define Acceptable Landing System Performance

Table 1 Summary of Airworthiness Requirements and Associated Equivalent Safety Criteria

General Condition	FAA Criteria	EASA Criteria	Related Success Criteria
Nominal Performance	AC 120-28D Nominal Performance – Section 6.3.1	CS–AWO 131 Performance demonstration AMC AWO 131 Performance Demonstration	Demonstrate equivalent or better performance under nominal conditions. (All variables varying across entire range). Meet 10^{-6} box
Malfunction Condition	AC 120-28D Performance with Malfunction – Section 6.4.1	CS AWO 161 – General (appears to apply but is less specific than FAA criteria as to what constitutes 'safe')	For all failures with probability > 10^{-9} demonstrate safe landing -> Land in box (with probability 1) – given environment and other variables „nominal'.
Limit Condition	No analogous requirement	EASA CS AWO 131 (c) – Performance Demonstration Limit case conditions	Demonstrate performance when one of the variables is at its "most critical value" while the others vary in their expected manner – Land in defined box with 10^{-5} -> Conditional probability approach

The three general conditions determine the kind of model that will need to be used for performance demonstrations. In general a suitable signal model must have the following capabilities:

- Produce representative errors (magnitude and spectral content) under nominal (fault-free) conditions. This includes nominal noise and other routine events like step errors due to geometry changes etc.
- Produce representative errors (magnitude and spectral content) under nominal (fault-free) conditions with an error representative of an NSE limit condition applied additively.
- Produce errors (magnitude and dynamics) representative of anticipated system malfunction modes.

In order to be representative, the performance demonstration encompasses various expected operational conditions in terms of aircraft configurations including aircraft weight and center of gravity location, flaps configuration and altitude. The performance demonstration also includes environmental parameters like wind or runway configuration.

As described in [25], in addition to the successful demonstration of aircraft landing in the box safely, several other parameters including impact on the crew workload must be assessed. We can note the ability of the pilot in command to identify the failure condition effect and to react appropriately, in compliance with the regulation. In addition, aircraft reaction in terms of control and guidance and cockpit effects must be adequate and timely.

The other objective of the airworthiness assessment is to provide a safety classification for the failure according to [26] and [27] and to verify that the classification of the failure (Minor, Major, Hazardous, Catastrophic) is in accordance with the failure probability.

More particularly, some parameters are quantitatively evaluated. These are longitudinal and lateral position at touchdown and during rollout, aircraft vertical speed at touchdown, aircraft attitude, speed and yaw rate during landing and rollout, aerodynamic surface deflection and margin with regard to the obstacle clearance surface. If one of these criteria is not met, either an airborne system design like a mitigation or a monitor will be required to mitigate the effect of the failure, or a change if possible in the probability of failure occurrence will be required. The overall evaluation process is illustrated below in Figure 2

One example among these criteria evaluated during ILS Category III airworthiness demonstration is the non penetration of a 1:29 slope boundary upon system failures, as defined in [28] and [29] and illustrated below in Figure **3**. This slope provides a margin against the obstacles, to enable the pilot or the aircraft to recover from a failure erroneously guiding the aircraft downward, all other conditions being nominal. But, because, GBAS is a rectilinear system, compared to the ILS system being angular, and due to the specificities of GBAS failure characteristics in terms of magnitude and dynamics, new or adapted criteria should be developed, ensuring safe landing in the most limiting case.

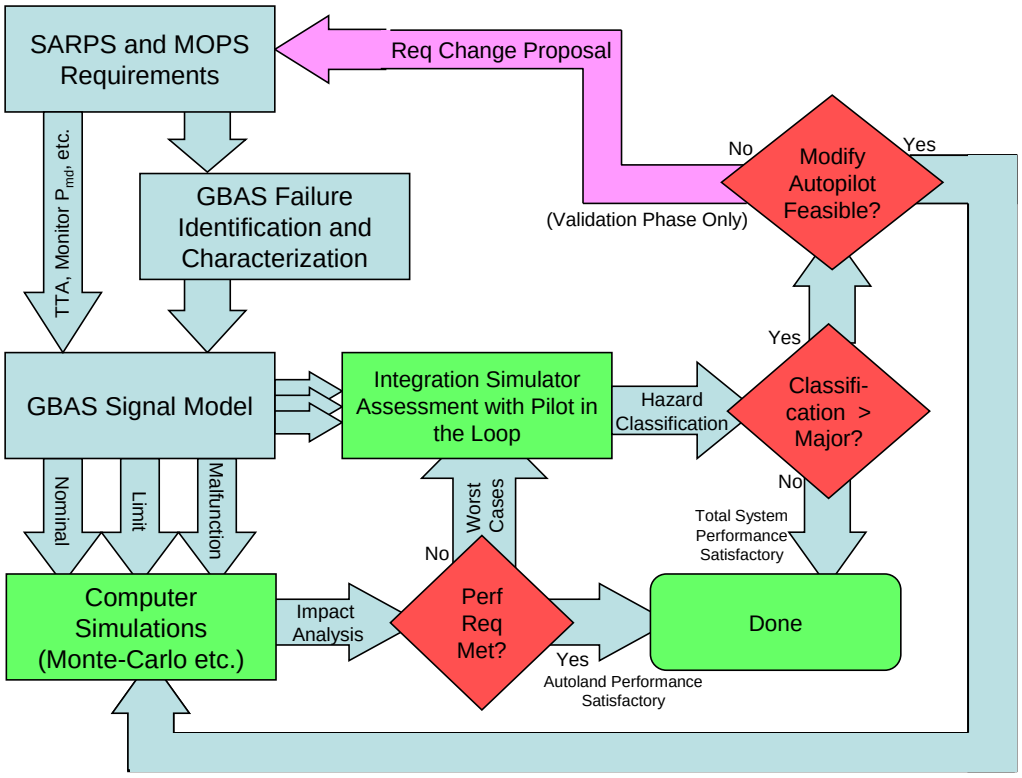

Figure 2: Precision approach failure assessment process

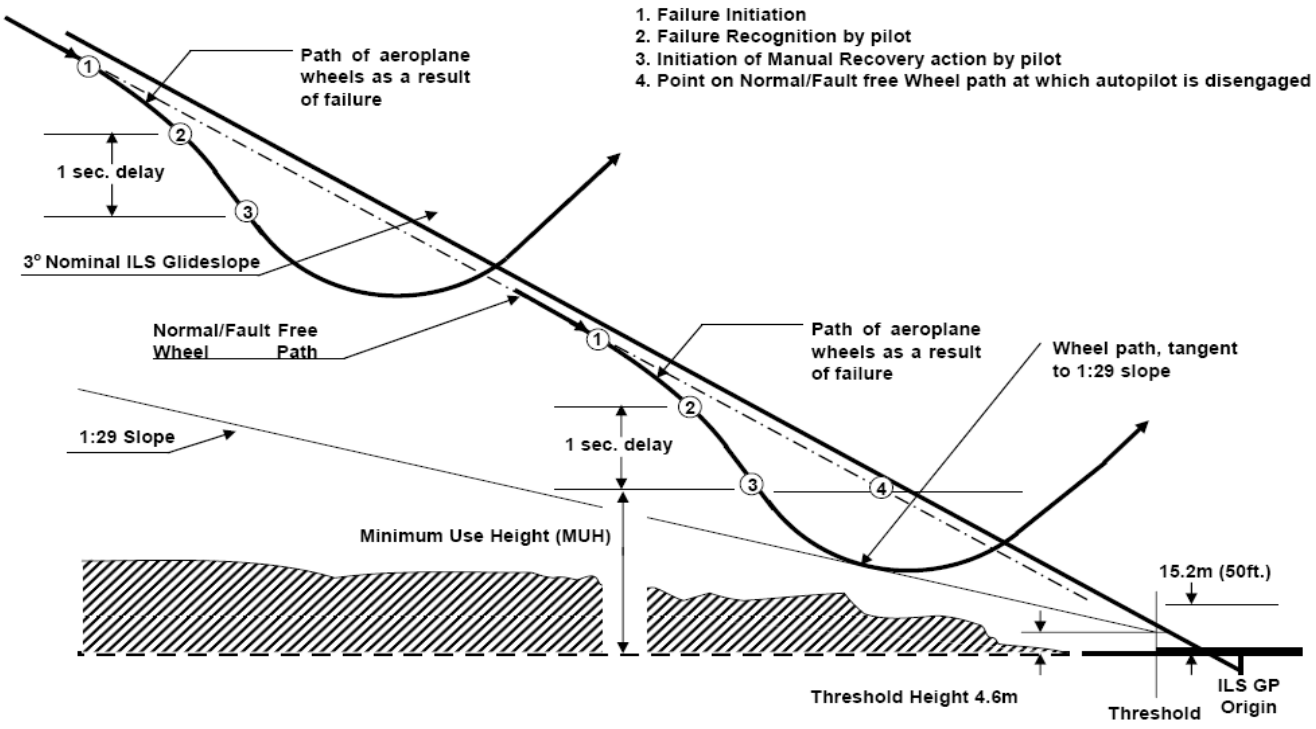

Figure 3: 1:29 slope penetration boundary

One new criterion currently under consideration (can be found in [30]) would include the combination of system and signal-in-space failure effects having a probability > 10^{-9} to demonstrate an absolute margin against obstacles below the flight path, known as the 1:50 slope. By the most limiting case, we mean the case where approach parameters are set at values which will have the most impacting effect on the flight guidance system, for instance smallest flight path angle or most critical aircraft configuration.

More particularly, types of failures that would be combined include ranging source failures, reference receiver failures and airborne system failures but not ionospheric anomalies. Indeed, since the prior probability of ionospheric anomalies cannot be well quantified, their effect on the aircraft landing performance will be evaluated separately.

GBAS Fault Modes

For a GBAS system three general classes of faults have been identified:

1. A satellite ranging sources failure
2. Failure of a single reference receiver
3. An ionospheric anomaly

The peak magnitude and effective threshold for error that persists post monitoring differs between these three fault types. The model proposal now gives information related to computing the maximum error and effective threshold for each fault type in terms of geometry screening factors applied by the airborne equipment. In this way, the airframe integrator can set the fault model to produce the appropriate sized errors given the specifics of the integration (i.e. the geometry screening factors.)

The maximum error that can be expected with a probability of greater than 10^{-9} is relevant for testing a landing system in the presence of a malfunction as defined in [8] and [9].

The effective threshold is relevant because the 'limit case' conditions as discussed in the GBAS GAST D concept paper [2] are based on the point of peak error probability which is at or just below the effective threshold for the monitor. Hence, the effective threshold relates to the size of an error that may need to be used in a limit case demonstration for this fault type as defined in [9].

GBAS FAULT MODEL

The effect of GBAS faults is modeled as a ramp error with characteristics as illustrated in Figure 4. The effect of a malfunction is modeled as a ramp, with a start time, a ramp rate and a total exposure time, Tmax. The maximum value of the ramp depends on the ramp rate and Time to Detect (TTD). The ramp is assumed to increase to the level of the Effective Alert Limit and then to exceed that value for a period equal to the Time-to-detect and mitigate the failure. The erroneous satellite is isolated and the error returns to the nominal value (i.e. the fault error is set to zero). The effect at the output of the receiver is either that the fault error returns to zero and the noise model produces only nominal errors or that the guidance signal is lost (e.g. the output of the receiver is flagged as unusable).

The Model may alternatively produce step errors where the maximum change in error due to the step is specified rather than the ramp rate.

It must be noted that fault errors are modeled separately from nominal noise errors and added to nominal noise errors where appropriate.

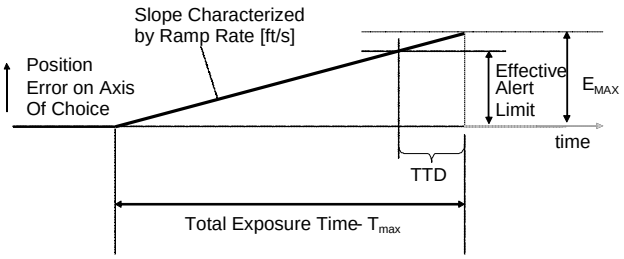

Figure 4 Malfunction Transient

A previous study [16] considered the historical record of documented satellite failures and concluded even without considering the ground station specific failures, a GBAS system could be exposed to transient ramps in pseudorange of virtually any slope. The augmentation data from the ground station may compensate for pseudorange ramp errors, but due to sampling rates and time to detect and mitigate the errors, the airborne equipment could output some transient errors driven by the pseudorange ramps. In the worst case, these transients would have a duration defined by the maximum time to detect and mitigate the error. The malfunction model proposed is based on a model of a failure in progress that is assumed to be a ramp with an arbitrary slope from near zero (i.e. essentially a bias over an approach) to near infinite (i.e. a step change). The magnitude of the error at the end of the slope will depend on the monitoring performed by the ground station and in particular on the minimal detectable error (the threshold) and the steepness of the slope combined with the time to detect (the overshoot).

As mentioned above, it is assumed that the GBAS system meets its requirements and either indicates the failure exists or removes the effect after no longer than the TTA

allocated to the ground segment. The possibility of data link missed messages is also considered to determine the maximum exposure interval for the airplane (referenced to the output of the GBAS receiver).

Ramps and steps are believed to be sufficient as models for failures based on the observed satellite failure characteristics. A more recent study performed by Honeywell [31] reviewed the expected fault modes of a GBAS and concluded that every fault mode but excessive acceleration can be modeled conservatively as a ramp. The exception to this rule is excessive acceleration which is expected to be second order (or quadratic) for the duration of the failure before it is detected and mitigated by the ground segment. Because the proposed failure model includes the entire family of ramp rates (from 0 to infinite), then for any postulated constant acceleration error, a similar ramp error can be found that causes the error to cross the threshold (i.e. minimum detectable error) at the same time and which results in an error of the same magnitude at the end of the time to detect. This situation is illustrated in Figure 5.

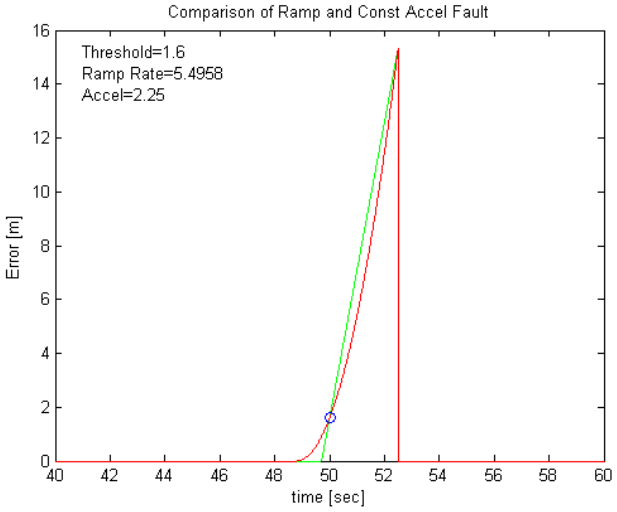

Figure 5 Comparison of Ramp Error and Similar Constant Acceleration Error

The response of an airplane to a steep ramp resulting in an error as large as or larger than the error that would be reached with the constant acceleration function in the same exposure interval should be as bad as the response to constant acceleration error. (The constant acceleration error simply looks like a steeper ramp with a shorter duration). To illustrate this further, consider the spectral content of ramp errors and constant acceleration errors. Figure 6 shows the ramp error and similar constant acceleration error from Figure 5 along with the Power Spectral Density (PSD) of each waveform. Note the similarity of the PSDs. Similarly Figure 7 compares the PSDs for a whole family of ramp errors and their associated power spectral densities. The ramp family can produce errors with spectral content essentially identical to the constant acceleration family.

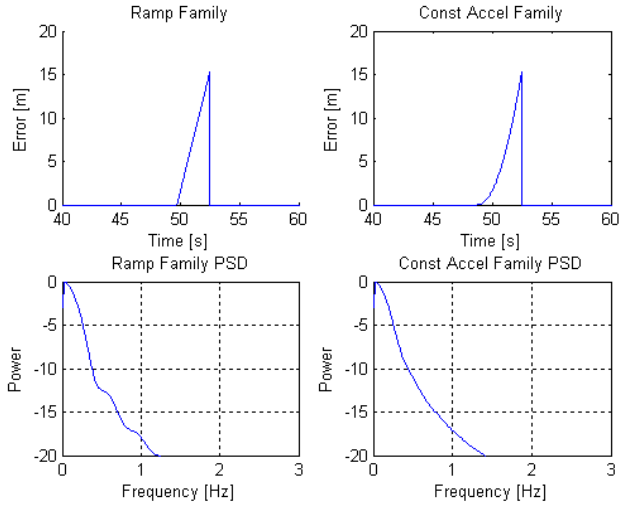

Figure 6 Comparison of PSD for Ramp Error and Similar Constant Acceleration Errror

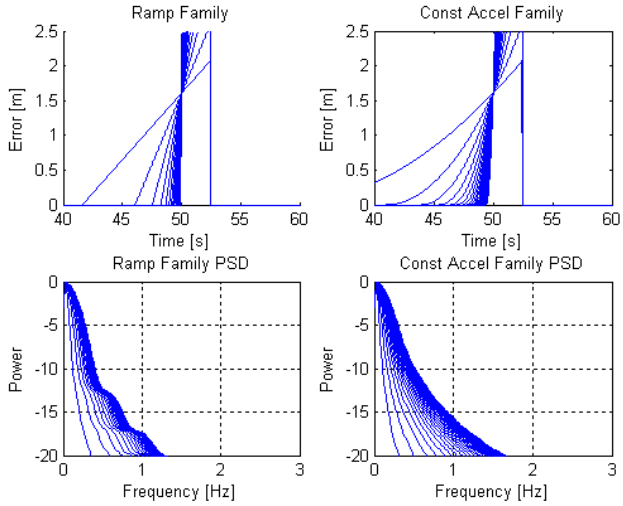

Figure 7 Comparison of the PSD for a Whole Family of Ramp Errors and the Associated Similar Constant Acceleration Errors

Figure 8 further illustrates the relative effect of ramp and constant acceleration errors when the airplane response is considered. The errors in Figure 8 are filtered using the vertical Path Following Error filter as defined in ICAO Annex 10 [32]. The PFE filter was introduced for MLS as a means to isolate MLS errors that would be expected to result in displacement of the airplane (i.e. errors that the airplane may actually follow). This is essentially equivalent to modeling the airplane response as a second order Butterworth low pass filter with a cutoff of 0.3 rad/s. This is a very conservative and simple model of airplane performance as more modern autopilot systems

have a closed loop bandwidth that is much smaller. From Figure 8 it can be seen that the ramp error family can produce responses as severe as or more severe than the similar constant acceleration family.

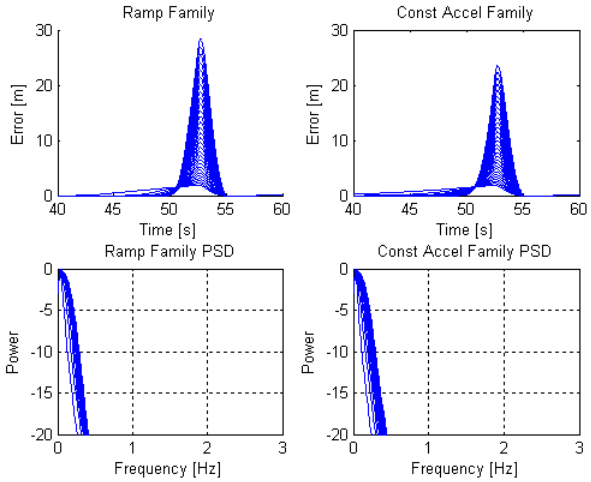

Figure 8 Comparison of Airplane Response to Family of Ramp Errors and Similar Constant Acceleration Errors

Airplane designs may also include anomaly detection features based on integration with inertial information. This would further mitigate the response of the airplane system to the transient errors. A full investigation of the impact of various error characteristics on anomaly detection designs is beyond the scope of this paper. However, a simple example is illustrated in Figure 9. In this simulation, the airplane response is modeled as a low pass filter in the same manner as before. However, prior to filtering a simple algorithm is applied where the instantaneous error rate is compared to a 1 m/s. threshold. Rates that exceed 1 m/s cause a detection and removal of the error (or loss of service). The errors with and without anomaly detection are shown in Figure 9. Note that although there are some differences as to when detections occur etc. the two families result in essentially identical envelopes of errors responses. In fact the peak errors are slightly larger for the ramp error family. Given all the considerations above, the ramp error model for GBAS faults is considered sufficient for testing airborne designs.

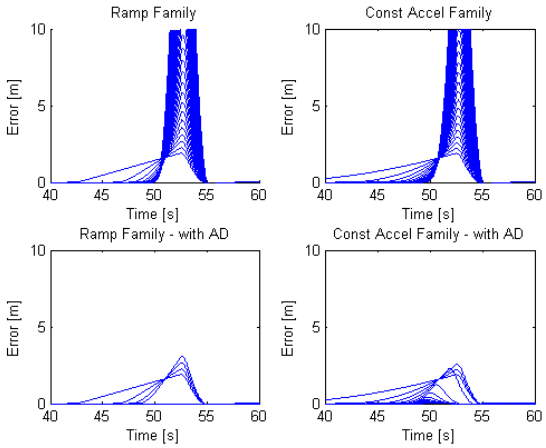

Figure 9 Comparison of Ramp Error Family and Constant Acceleration Error Family with Simple Anomaly Detection

As mentioned above the peak magnitude of the error (E_{max}) and the Effective threshold are different between the different fault types. For each fault mode E_{max} and the effective threshold can be related by geometry screening parameters that are defined by the aircraft integrator. Reference [33] gives a detailed derivation of the error characteristics for the single reference receiver failure. References [34] and [35] discuss the analysis done to validate the ionospheric anomaly monitoring. The maximum error that can occur in the pseudorange domain due to a satellite ranging source failure is specified directly in the proposed SARPS requirements (reference [1] section 3.6.7.3.3.2). The analyses for each of these fault modes are discussed in the following section.

SATELLITE RANGING SOURCE FAILURES

Satellite failures that cause the measured pseudo range to deviate from its intended value are typically not a safety risk in a differential system but certain satellite failure modes may create unacceptable differential errors due to their particular nature. These are referred to as satellite ranging source faults and the GAST D standard identifies the following 4 different types: excessive acceleration, excessive carrier code divergence, excessive ephemeris errors and signal deformation.

For signal deformation the transmitted C/A code is distorted due to a fault condition in the satellite. This in turn leads to a deformation of the correlation peak. The deformation of the correlation peak will be modified by the front end filtering and the resulting code tracking further depends on the correlator type and correlator spacing. DO-253C [36] contains the constraint regions associated with these airborne characteristics. The typical outcome of signal deformation is that the airborne and ground errors differ, resulting in a differential error. If the

deformation is present as the satellite is acquired the ground will detect it and the satellite will be excluded from use. The scenario that is of interest for the airworthiness assessment is the transient case where there is a sudden failure in the satellite that instantaneously exposes the differential system to a deformed correlation peak. This results in a differential pseudorange step (dpr) that due to the smoothing in turn will result in an exponential step response

$$E_R(t)= (1-e^{-at}) \text{ dpr}$$

where dpr, in the range 1 m to 35 m, determines the initial ramp rate and $a=1/\tau = 1/30$ sec. This step response together with the 10^{-9} 1.6 m limit associated with the malfunction condition are illustrated in Figure 10

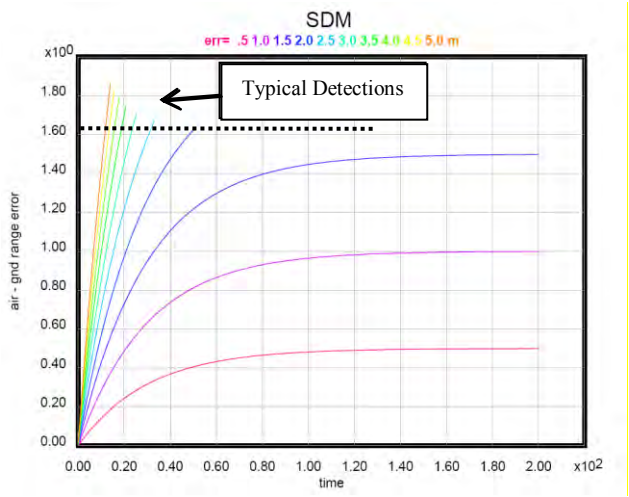

Figure 10 Signal Deformation Malfunction Transient

Figure 10 shows how the 10^{-9} error would exceed the 1.6 m due to the 2.5 sec time to alarm. The larger the slope the further it goes in 2.5 sec. Initially this error can be approximated by a ramp

$$\text{ramp}(t) = a \times \text{err} \times t$$

but later it tapers off in magnitude and rate.

The excessive acceleration affects the airborne equipment because of the unavoidable delays in the differential correction broadcast. An instant acceleration in the signal will immediately be sensed by the airborne receiver and cause an error in the estimated airplane position. The ground station will sense the same acceleration but due to communication and processing both in ground system and airborne system there is a nominal delay of τ seconds (2.5 sec). The GBAS standard includes a differential correction rate used for linear extrapolation to the current time that reduces the error due to the delay but there is no means of including the effect of an acceleration in this extrapolation. The pseudorange acceleration, *A*, caused by the fault is unlimited in magnitude. The error is $0.5 \cdot A \cdot t^2$ for t in the interval $[0,\tau]$. After that, $t \geq \tau$, the error is constant and equal to $0.5 \cdot A \cdot \tau(\tau+0.5)$ or the satellite excluded based on the requirement that $E_R = 0.5 \cdot A \cdot \tau(\tau+0.5)$ meets the p_{md} constraint (10^{-9} at 1.6 m). The extra 0.5 sec term relates to the way the correction rate is formed based on a difference of two differential corrections and then used in the extrapolation. The resulting errors are shown in Figure 11 for accelerations in the range 0.1 to 1 m/s^2.

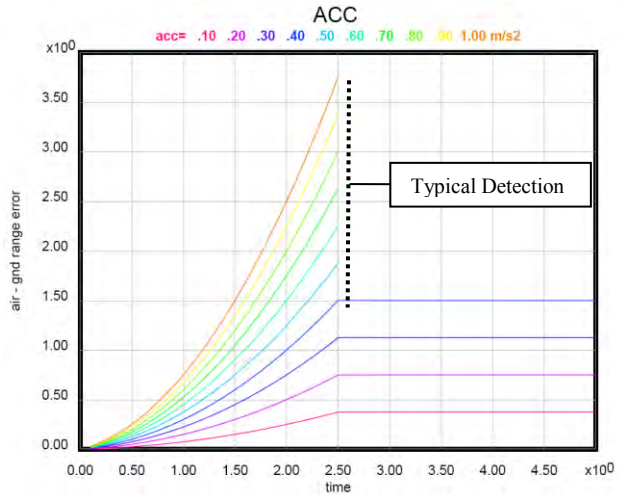

Figure 11 Excessive Acceleration Range Error

The major reason for the carrier code divergence (CCD) error is that the airborne system (according to DO-253C) may use a time variant time constant equal to elapsed time from initialization for the first 30 seconds instead of a fixed time constant of 30 sec (after 30 sec the airborne is required to use a fixed time constant of 30 sec). The fault mechanism is best described by the Laplace block diagram in Figure 12.

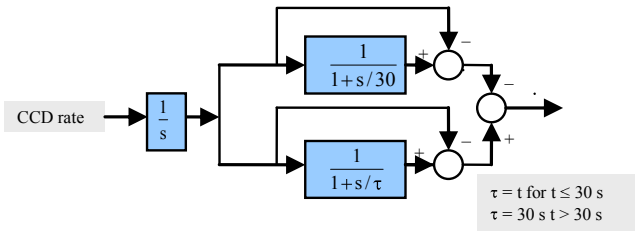

Figure 12 Excessive CCD Range Error

As can be seen the fault mechanism has no longer any impact if the fault is occurring 30 sec after initialization since the time constants are then the same. The impact of a carrier code divergence rate (in cm /s) can be simulated based on the block diagram and the difference between ground and air is shown in Figure 13 assuming divergence starts immediately after initialization of the

smoothing filter in the airborne system. If the CCD rates are carrier driven (code is correct while carrier is drifting), rates greater than 40 cm/s typically do not pass the rate and acceleration monitors. However, if the CCD rates are code driven errors may result as shown in Figure 13. It is also clear from Figure 13 that the error cannot be limited to 1.6 m if the rate is increased indefinitely. A MOPS (DO-253C) change has been identified to delay the incorporation of satellites into the guidance solution until 30 seconds has passed to assure the SDM monitor has enough time to exclude a satellite when the fault occurs just before initialization. The CCD fault impact is similar to the SDM impact in that it starts out as a ramp and then reduces in size and rate and its impact can therefore conservatively be modeled by a ramp. Note that if the incorporation of satellites into the guidance solution is delayed then the fault may manifest itself as a step rather than a ramp (see grey line marking the 30 delay in Figure 12).

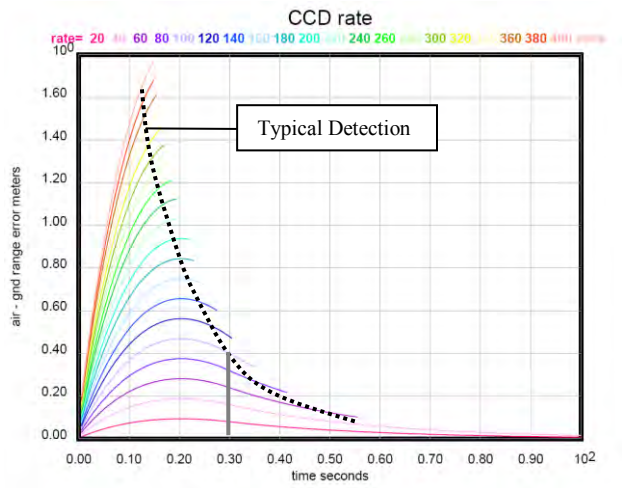

Figure 13 CCD Errors

The excessive ephemeris fault is currently split into 3 categories A1, A2 and B. In category B the broadcast ephemeris data is in error due to an OCS-blunder or satellite glitch. The ephemeris monitor always checks the satellite positions in the section of the orbit that will be used in the ground calculations before they are used so that the fault is detected before any differential corrections affected by the fault, are broadcast. The core threat in category A1 is broadcast of stale (unchanged) ephemeris parameters after a delta-V maneuver out of view (satellite healthy at acquisition). The detection of the fault is part of the acquisition process and no differential corrections will be broadcast if a fault is detected.

The threat in category A2 is an unannounced delta-V maneuver in view. In this case the fault cannot be detected in advance. The satellite is drifting off and at some point the satellite position error will be detected. The satellite needs to be at least several kilometers off to produce a 1.6 m radial error at 10 km. This fault impact can consequently be modeled as a slow ramp.

GROUND STATION SINGLE REFERENCE RECEIVER FAILURES

Appendix A gives a derivation of the Probability of missed detection (P_{md}) for the Reference Receiver Fault Monitor (RRFM) as defined in the MOPS [36] and supported by SARPS requirements [37]. The derivation is then used to compute the largest error that a user can be exposed to with a probability of greater than 10^{-9}. It is anticipated that such an error characterization would be used in assessing airplane landing system performance given a GBAS malfunctions (i.e. a worst case single reference receiver failure in this case).

The derivation in Appendix A shows that if no additional geometry screening is imposed by the airborne equipment other than VPL<VAL = 10 meters, then the worst case error that can exist with a probability of greater than 10^{-9} after RRFM monitoring is 9.35 meters in the vertical. Also assuming no additional geometry screening, the RRFM provides a maximum effective threshold of 6.5 meters. However, these worst case conditions are driven by cases where only 2 reference receivers are used which is probably not a realistic scenario. Appendix A also includes a discussion of possible geometry screening that might be imposed by the airborne equipment with little or no impact on availability. With appropriate geometry screening, much smaller values of the maximum error and effective thresholds for this fault mode can be obtained.

The lateral error situation is similar in that if no additional geometry screening is imposed, then the worst case error that can exist with a probability of greater than 10^{-9} after RRFM monitoring is 35.9 meters in the lateral direction. Also, again, assuming no additional geometry screening, the RRFM provides a maximum effective threshold of 24.5 meters in the lateral direction. These worst case conditions are driven by cases where only 2 reference receivers are used which is probably not a realistic scenario. The appendix shows that geometry screening can be employed to substantially lower the worst case error (and effective threshold). The most straight forward solution is to geometry screen based on the computed threshold $T_{B\_air\_lat}$. If this approach is chosen, then the maximum error that can persist with a probability of greater than $1x10^{-9}$ can be read directly from the graph in Figure 22 (in Appendix A) for any particular limit imposed on $T_{B\_air\_lat}$.

IONOSPHERIC ANOMALIES

Ionospheric anomalies caused by solar storms can cause large changes in error over relatively short baselines [38, 39, 40, 41, 42]. A significant amount of effort has gone into implementing mitigations for the potential errors that could be induced in a GBAS system by such ionospheric anomalies [43, 44, 45, 46, 47, 48, 49]. The mitigations introduced for GAST D include monitoring in the airborne equipment, improved monitoring in the ground subsystem, some GBAS siting constraints and a limitation on the range of ionospheric threats (i.e. a standardized threat space).

References [50] and [51] discuss the analysis done to validate the ionospheric anomaly mitigations. That analysis showed the largest error that can persist in the pseudorange after application of all of the iono-anomaly mitigation measures is 2.75 meters. Figure 14 shows the plot of the maximum error in the pseudorange domain for any phasing of airplane motion and front motion as a function of front speed relative to the reference pierce point after taking into account airborne CCD monitoring, position domain dual solution monitoring, and reference station monitoring of the absolute gradient between reference antennas. The effect of CCD monitoring in the reference subsystem is not taken into account in Figure 14 since it is not specified in the GAST D requirements. However, using an example design, only the shape of the maximum error curve is changed, and the peak value is unaffected.

Figure 15 shows the maximum rate of change of the vertical or horizontal position domain error due to ionosphere anomalies that can be experienced at any point during the approach up to the point of detection, if it occurs, for the same ionosphere anomaly monitors. The discontinuity at 1350 meters per second arises from an assumed threat space limitation that is assumed of 100 mm/km gradients for ionosphere front ground speeds greater than 750 m/s as is described in [1]. Pierce point motion is assumed at a shell height of 350 km to reach speeds of 600 m/s for a maximum front speed relative to the pierce point of the sum, or 1350 m/s. Note that for high relative speeds, the maximum possible error rate is driven by the initial carrier phase run-off and only persists for the time-to-detect. This rate approaches the product of the maximum gradient and the relative front speed in the range domain, multiplied by the position solution projection in the position domain.

For both Figure 14 and Figure 15, the airborne CCD monitor was assumed to detect after the test statistic has exceeded the threshold plus six times the noise standard deviation for up to a time-to-detect of 1.5 seconds to approximate a 10^{-9} probability of missed detection (P_{md}). The absolute gradient monitor was assumed to detect within the requirement of 1.5 meters divided by the threshold distance of 5 km, or 300 mm/km within 2.5 seconds. It has been shown that this is feasible with a missed detection probability approaching even 10^{-9} [34]. Finally, the position domain dual solution monitor was assumed to detect after the dual solution exceeded the required 2m threshold plus six times the standard deviation of the measurement noise to approximate a 10^{-9} Pmd. These are very conservative assumptions. The maximum position error rate due to ionospheric anomalies at a typical time of detection is less than one meter per second.

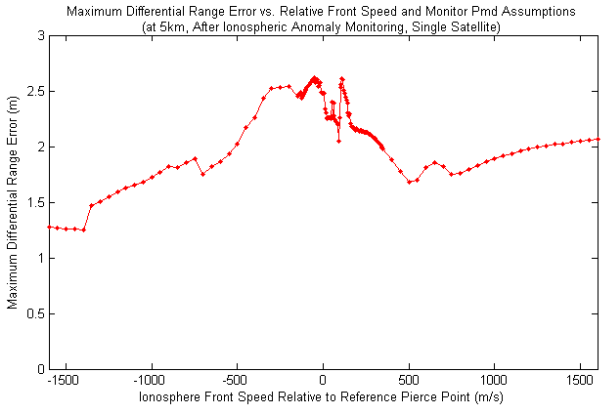

Figure 14 Maximum Range Errors Persisting after Ionospheric Mitigations

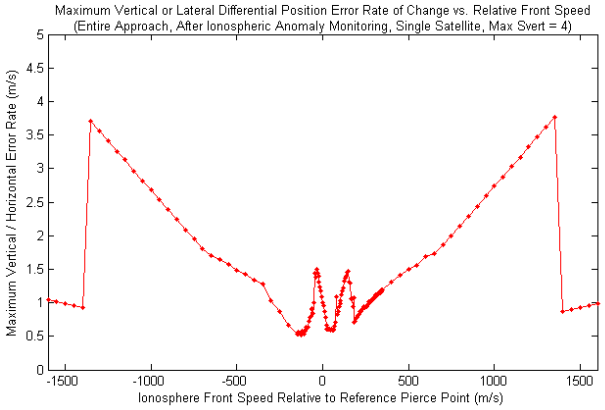

Figure 15 Maximum Rate of Position Errors During Approach or Until the Point of Detection

Ionospheric anomalies are caused by environmental factors such as space weather resulting from strong solar activity. They have been modeled for several parts of the world by a large international effort, to determine a practical and representative model that anyone could use for airworthiness demonstrations. Indeed, demonstrations supporting precision approach certification are anticipated to be performed once and for all airports with approaches targeted by the type certificate.

However, a lack of hindsight and a lack of sufficient

historical data prohibit using a statistical approach to demonstrate airworthiness during large ionospheric events. Indeed, precise environmental conditions and their associated probability of occurrence > or < 10^{-9} could not be determined for large peaks of errors that may be encountered by the aircraft. Assuming this phenomenon is obviously not caused by a system failure, is environmental (i.e. external to the GBAS system including the aircraft) and is not predictable, it has been found adequate to consider this phenomenon as a malfunction event from the airworthiness point of view. As a consequence, it is chosen to assess the aircraft airworthiness against this event with a deterministic approach.

Enhanced modeling of ionospheric anomalies including probability of occurrence could enable in the future the adoption of a statistical approach and incorporate it into Monte-Carlo simulations. In the meantime, improved monitoring capability and mitigation techniques should be associated with enhanced space weather prediction capability from a ground network, in order to warn crews when conditions might exceed the aircraft certificate envelope as it is done with large crosswind conditions.

GBAS FAULT MODEL SUMMARY

A summary of the parameters for the GBAS fault model is given in Table 2 and Table 3 for vertical and lateral errors respectively. Note that the characteristics of the fault (i.e. magnitude and effective threshold) are functions of geometry screening parameters, Svert S_{vert2}, S_{lat} and S_{lat2}. S_{vert} (S_{lat}) is the largest vertical (lateral) coefficient magnitude for any single satellite. S_{vert2} (S_{lat2}) is the largest sum of vertical (lateral) coefficient magnitudes for any two satellites. These parameters are set by the airframer to ensure that the maximum fault mode error magnitudes are acceptable given the airplane performance.

It is the airframer responsibility to determine the most critical altitude at which the failure needs to be injected as well as all the geometry screening parameters and thresholds that will impact the size of the errors.

Attention must also be paid to the way the GBAS receiver outputs the deviations from the intended flight path. Indeed, in the angular case for the glide slope, a failure injected as a ramp will not result in a ramp at the output of the GBAS receiver.

Table 2 Malfunction Transient Characteristics in the Vertical Direction

Fault Type	Service Type	Ramp Rates [m/s]	Effective VAL [m]	E_{max} [m]	Effective Threshold [m]
Ranging Source Failures	**GAST C**	**0 - ∞**	**10**	**Dependent**	**N/A**
	GAST D	**0 - ∞**	**1.6 × S_{vert}**	**Dependent**	**0.75× S_{vert}**
Iono Anomaly	**GAST C**	**[0 – 2]**	**N/A**	**10**	**N/A**
	GAST D	**[0 – 2]**	**N/A**	**[2.75] × S_{vert} [2.75]× S_{vert2}**	**N/A**
Single Ref Receiver Failure	**GAST C**	**0 - ∞**	**10**	**Dependent**	**N/A**
	GAST D	**0 - ∞**	**9.35 [note 1]**	**Dependent**	**6.5 [note 1]**

Note 1: These values are an absolute worst case assuming no geometry screening is done based on TB_air_vert or M. Only geometry screening of VPL<VAL=10m is assumed. Smaller maximum values can be obtained by using additional geometry screening per reference [52].

Table 3 Malfunction Transient Characteristics in the Lateral Direction

Fault Type	Service Type	Ramp Rates [m/s]	Effective LAL [m]	E_{max} [m]	Effective Threshold [m]
Ranging Source Failures	**GAST C**	**0 - ∞**	**40**	**Dependent**	**N/A**
	GAST D	**0 - ∞**	**1.6 × S_{lat}**	**Dependent**	**0.75× S_{lat}**
Iono Anomaly	**GAST C**	**[0 – 2]**	**N/A**	**40**	**N/A**
	GAST D	**[0 – 2]**	**N/A**	**[2.75] × S_{lat}** **[2.75] × S_{lat2}**	**N/A**
Single Ref Receiver Failure	**GAST C**	**0 - ∞**	**40**	**Dependent**	**N/A**
	GAST D	**0 - ∞**	**35.9 [note 1]**	**Dependent**	**24.5 [note 1]**

Note 1: These values are an absolute worst case assuming no geometry screening is done based on $T_{B\_air\_lat}$ or M. Only geometry screening of LPL<LAL=40m is assumed. If geometry screening of LPL<LAL=10m is applied, then the values for Effective LAL and Effective Threshold would be the same as the values given in Table 2 for Effective VAL and Effective threshold respectively. Smaller maximum values can be obtained by using additional geometry screening per reference [19] (e.g. a limitation on $T_{B\_air\_lat}$ or M).

CONCLUSIONS

This paper has reviewed the current state of development of a GBAS signal model which has been developed to support airworthiness assessments. In particular, the characteristics of anticipated fault modes have been explored. A simple ramp error model is proposed and the characteristics of the ramp errors as a function of aircraft integrator defined thresholds and geometry screening are presented.

The next step for this work is to have this model internationally recognized and accepted by airworthiness authorities in the frame of rulemaking activities, contributing to GBAS GAST D proof of concept and providing GBAS Category III certification baseline for aircraft manufacturers.

ACKNOWLEDGMENTS

The authors would like to acknowledge the many people whose efforts made this paper possible. The work described in this paper builds on the work done by many people over the course of many years. In particular, the authors would like to acknowledge the efforts of Christel Ravier, Diane Rambach, Barbara Clark, Sam Pullen, Boris Pervan, Lingan Satkunanathan, Gary McGraw, Pierre Neri, Christophe Macabiau, Young Nam, Tom Zalesak, and Mike Braasch, all of whom have contributed at one point or another to the modeling of GBAS errors.

APPENDIX A

This appendix explains how to determine Pmd for the RRFM and how to compute the largest error that a user may see with a probability of greater than 10^{-9} due to failure of a single reference receiver when using GAST D. The derivation draws heavily from references [53] and [54].

Review of Monitor and Computation of Pmd Performance

Recall from the MOPS [36] that the form of the Monitor is (considering only the vertical for simplicity's sake):

$$\left|B_{j\_Apr\_vert}\right| + D_V \le T_{B\_air\_vert} \quad [1]$$

where

$$B_{j\_Apr\_vert} = \sum_{i=1}^{N} S_{Apr\_vert,i} B_{i,j} \quad [2]$$

and

$$T_{B\_air\_vert} = K_{ffd\_B}\sqrt{\sigma^2_{B\_vert} + \sigma^2_{D_V}} \quad [3]$$

and finally,

$$\sigma^2_{B\_vert} = \sum_{i=1}^{N} \frac{S^2_{Apr\_vert,i}\sigma^2_{pr\_gnd\_100,i}}{U\_} \qquad [4]$$

So, it can be seen that the instantaneous geometry affects both sides of equation [1]. However, for any given geometry, the size of $T_{B\_air\_vert}$ is known. Therefore the probability of missed detection can also be computed if the distribution of the noise on the detection statistic in the faulted circumstance is known.

The probability of missed detection P_{md} as a function of the size of the bias in the vertical error E_V due to the single RR fault is given by:

$$P_{md}(E_V) = \text{Prob}\{B_{j,vert}(E_V) + |V_{diff}| \le T_{BAC}\} \qquad [5]$$

Where V_{diff} is the difference between the 30 second smoothed position solution and the 100 second smoothed position solution in the vertical direction. Consequently,

$$D_V = |V_{diff}| \qquad [6]$$

Under the assumption that $B_{j,vert}$ and V_{diff} are independent Gaussian random variables the P_{md} for the monitor can be computed by:

$$P_{md}(E_V) = \int_0^{\infty} \int_0^{T_{BAC}-y} p_{Bmd}(x, E_V)\, p_{D_V}(y)\, dx dy \qquad [7]$$

Where $p_{Bmd}(x,E_V)$ is the probability density function (pdf) of $|B_{j,vert}(E_V)|$ in the faulted circumstance given by

$$p_{Bmd}(x, E_V) = \begin{cases} x \ge 0; dnorm(x, E_V, \sigma_{Bmd}) + dnorm(-x, E_V, \sigma_{Bmd}) \\ x < 0; 0 \end{cases} \qquad [8]$$

Where $dnorm(x,\mu,\sigma)$ is the Gaussian pdf

$$dnorm(x, \mu, \sigma) = \frac{e^{-\frac{(x-\mu)^2}{2\sigma^2}}}{\sqrt{2\pi}\sigma} \qquad [9]$$

It has been previously shown [53, 54] that in the faulted circumstance σ_{Bmd} is given by

$$\sigma_{Bmd} = \frac{\sigma_{B,vert}}{\sqrt{M}} \qquad [10]$$

Since D_V is the magnitude of V_{diff}, $p_{DV}(y)$ is given by

$$p_{D_V}(y) = \begin{cases} y \ge 0; dnorm(y, 0, \sigma_{D_V}) + dnorm(-y, 0, \sigma_{D_V}) \\ = 2 \times dnorm(y, 0, \sigma_{D_V}) \\ y < 0; 0 \end{cases} \qquad [11]$$

The expression for computing $P_{md}(E_V)$ given by equation [7] is exact. However, it involves double integration of pdfs, which is inconvenient and time consuming. Therefore, a bounding approximation for $P_{md}(E_V)$ can be formulated by making the following observation. Since D_V is always positive, including D_V in the decision statistic actually decreases the effective threshold (and thus the probability of missed detection) for a given size of $|B_{j,vert}(E_V)|$. Therefore, ignoring the effect of D_V in the decision statistic (but not in the setting of the threshold T_{BAC}) gives an upper bound on $P_{md}(E_V)$. The resulting approximation involves only a single integration

$$P_{mdApprox}(E_V) = \int_0^{T_{BAC}} p_{Bmd}(x, E_V)\, dx \qquad [12]$$

A plot of both $P_{md}(E_V)$ and $P_{mdApprox}(E_V)$ vs E_V is given in Figure 16. Note that the approximation provides a close upper bound. The value of E_{Vbnd} is only 0.25 m to 0.5 m larger than the value of E_V for which $P_{mdApprox}(E_{Vbnd}) = P_{md}(E_V)$.

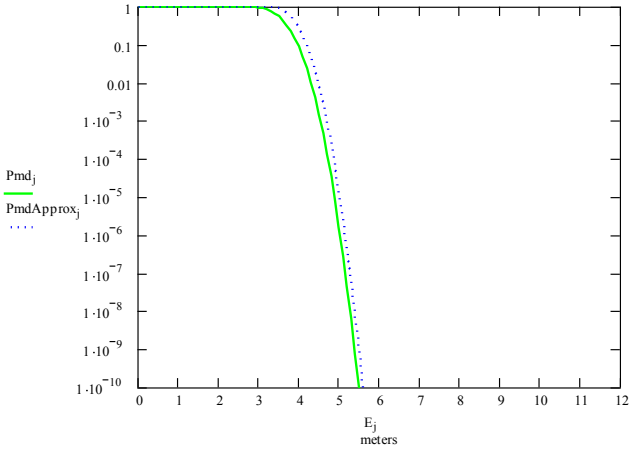

Figure 16 Single RR Fault Airborne Monitor P_{md} – Exact and Approximation

For a given aircraft integration, a largest tolerable error exists such that any larger error would result in an unacceptable landing. A potential geometry screening is implied by equation [12]. For a given geometry, the probability of the maximum tolerable E_V can be determined by the relationship in [12]. If the $P_{md}(E_v)$*a priori probability is greater than $1x10^{-9}$, then the geometry is unacceptable. Since the maximum a priori probability of a single reference receiver fault is (now) specified as $1x10^{-5}$/approach, then if $P_{md}(Ev)>1x10^{-4}$, the geometry is unacceptable. Thus the

RRFM monitor can be used as a means of geometry screening.

Computation of the Maximum Error Post Monitoring

For the purposes of airworthiness certification, we are interested in computing the largest error that can occur and be undetected with greater than 10^{-9} probability. To determine this we need to determine the largest value of the threshold $T_{B\_air\_vert}$ that can result from any geometry and then the largest value of $\sigma_{B,vert}$ in equation [4]. To do this we follow the derivation given first in [53]. A complete derivation with computations based on slightly different assumptions is given in [33].

Figure 21 shows a plot of the Pmd for RRFM given the maximum $T_{B\_air\_vert}$ and $\sigma_{B,vert}$ as computed in reference [33] for M=4 and VAL = 10 m. The computation of the curve is per equation [12]. Also shown on the plot is the maximum E_v (Max E_v) where $P_{md}(E_v)$×(priori probability of a single reference receiver) is equal to 1×10^{-9}. For GAST D the prior probability is required to be 1×10^{-5} or smaller. Hence the required $P_{md}(E_v)$ is 1×10^{-4} or smaller. So, the maximum size of an error induced by failure of a single reference receiver that can exist after monitoring with a probability of 1×10^{-9} is 4.45 meters.

Figure 18 shows the computation of $T_{B\_air\_vert}$ and Max E_v for other values of VAL. It can be seen that more aggressive geometry screening (i.e. VPL≤ VAL < 10 meters) results in smaller maximum detection thresholds ($T_{B\_air\_vert}$) and consequently smaller Max E_v. This illustrates the VPL geometry screening is one possible method to reduce the maximum error and effective threshold for RRFM.

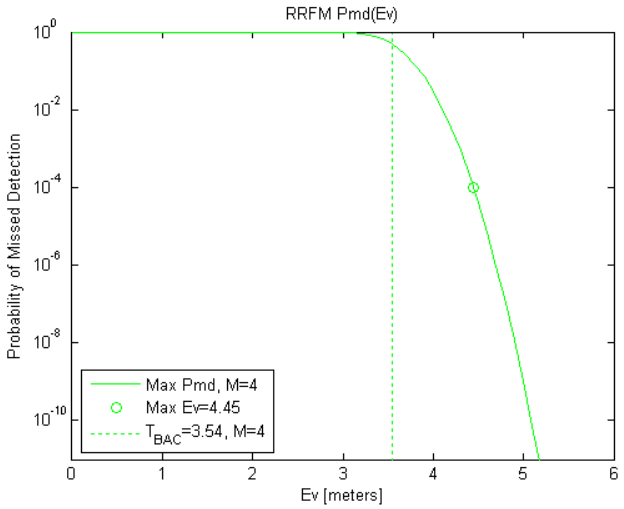

Figure 17 $P_{md}(E_v)$ for RRFM given M=4 and the Assumptions Listed in Reference [33]

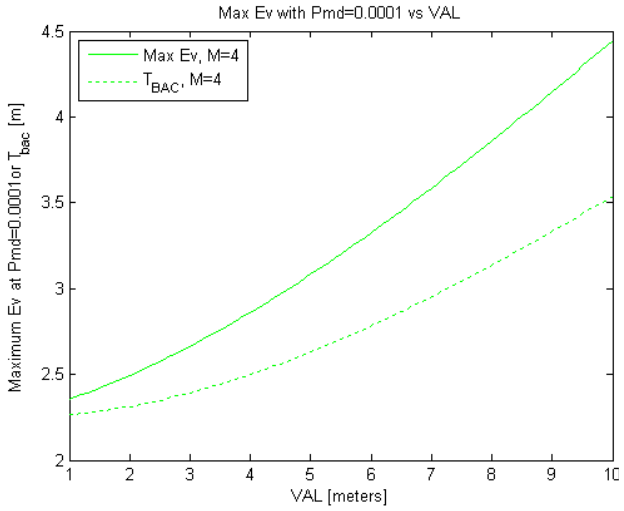

Figure 18 Max Ev and $T_{B\_air\_vert}$ as a function of VAL

Figure 19 shows the $P_{md}(E_v)$, $T_{B\_air\_vert}$ and Max E_v, for M=2, 3 and 4. Note that as the number of active reference receivers decreases, the detection threshold and Max E_v are increased substantially. For normal operations with a GAST D ground station, M=3 is considered a probable situation. Continued operations with M=2 seems less likely. (It is not likely the ground station can meet the continuity requirements with only 2 receivers, so it may have to annunciate GAST C as the status when it goes to 2 receivers.) However there is nothing in the currently proposed standards explicitly precluding the use of a signal from a FAST D ground station which has only 2 active reference receivers.

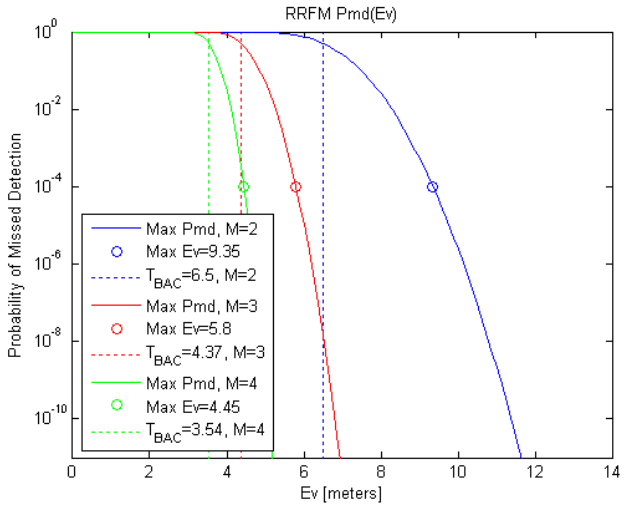

Figure 19 Pmd for RRFM as a function of M and the Assumptions Listed in Reference [33]

Figure 20 shows the computation of $T_{B\_air\_vert}$ and Max E_v for other values of VAL and M=2, 3 or 4. Again, more

aggressive geometry screening (i.e. VPL≤ VAL < 10 meters) results in smaller maximum detection thresholds ($T_{B\_air\_vert}$) and consequently smaller Max E_v for a given M. This illustrates that not only is VPL geometry screening one possible method to reduce the maximum error and effective threshold for RRFM but that it could be used in conjunction with geometry screening based on M.

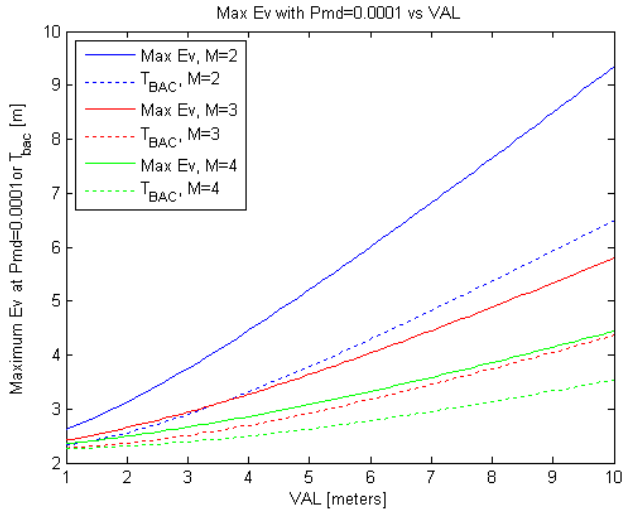

Figure 20 Max Ev and $T_{B\_air\_vert}$ as a Function of VAL and M

It is important to understand that the methodology used to compute the maximum $T_{B\_air\_vert}$ and Max E_v above is a conservative approximation based on some assumptions about the relative levels of noise. To check the veracity of this approximation a simulation was constructed. The details of the simulation and the results are given in [33]. The results of the simulation were in close agreement with the results obtained from the approximation.

$T_{B\_air\_vert}$ and $\sigma_{B,vert}$ are related per equations [3]. Consequently, for a given value of σ_{D_V}, $\sigma_{B,vert}$ is a direct function of $T_{B\_air\_vert}$:

$$\sigma_{B\_vert} = \sqrt{\left(\frac{T_{B\_air\_vert}}{K_{ffd\_B}}\right)^2 - \sigma_{D_V}^2} \qquad [13]$$

Since, Max E_v is a function of $T_{B\_air\_vert}$ and $\sigma_{B,vert}$, this suggests that the magnitude of Max E_v can be limited directly by geometry screening with $T_{B\_air\_vert}$. Substituting equations [8], [10] and [13] into equation [12] we obtain:

$$P_{mdApprox}(E_V) = \int_0^{T_{BAC}} \left(dnorm\left(x, E_V, \sqrt{\frac{1}{M}\left(\left(\frac{T_{B\_air\_vert}}{K_{ffd\_B}}\right)^2 - \sigma_{D_V}^2\right)}\right) + dnorm\left(-x, E_V, \sqrt{\frac{1}{M}\left(\left(\frac{T_{B\_air\_vert}}{K_{ffd\_B}}\right)^2 - \sigma_{D_V}^2\right)}\right)\right) dx$$

[14]

Max $E_v(T_{B\_air\_vert})$ can be determined by solving the above equation for

$$P_{mdApprox}(E_V) = \frac{10^{-9}}{P_{prior}} = \frac{10^{-9}}{10^{-5}} = 10^{-4} \qquad [15]$$

Figure 21 shows a plot of E_v as a function of $T_{B\_air\_vert}$ assuming the prior probability of a reference receiver failure is $1x10^{-5}$. There are still 3 different curves, representing the cases of M=2, 3 and 4. (Examination of equation [14] reveals that Max $E_v(T_{B\_air\_vert})$ depends on M). The maximum values of $T_{B\_air\_vert}$ that should ever be encountered for each M are also indicated on the graph. An airframe integrator could decide to implement a limit on the acceptable $T_{B\_air\_vert}$ and thereby limit the Max E_v. For example, if the maximum $T_{B\_air\_vert}$ was set to 4.5 meters, then the Max E_v given M=2 would be about 6 meters. The value of 4.5 meters for $T_{B\_air\_vert}$ is somewhat above the largest value of $T_{B\_air\_vert}$ that should ever be encountered if M=3 (based on both the approximation and simulation results above). Hence, geometry screening with $T_{B\_air\_vert} \leq$ 4.5 meters should never impact availability if the ground station has at least 3 active reference receivers (which should virtually always be true).

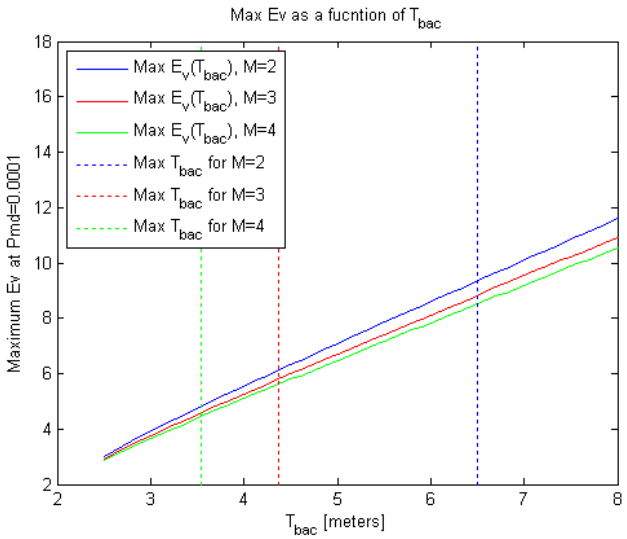

Figure 21 Max E_v as a Function of $T_{B\_air\_vert}$ (or T_{bac})

Reference [33] contains a derivation for the maximum error in the lateral direction, E_L, similar to that given above for E_V. The results of that analysis are repeated here for convenience. Figure 22 shows a plot of Max E_L as a function of $T_{B\_air\_lat}$ for the cases of M=2, 3 and 4. Note The figure clearly shows that the Maximum E_L that could be encountered with a probability of greater than $1x10^{-9}$ is limited for a given $T_{B\_air\_lat}$. Hence, a geometry screening based on $T_{B\_air\_lat}$ can be used to limit the Maximum E_L.

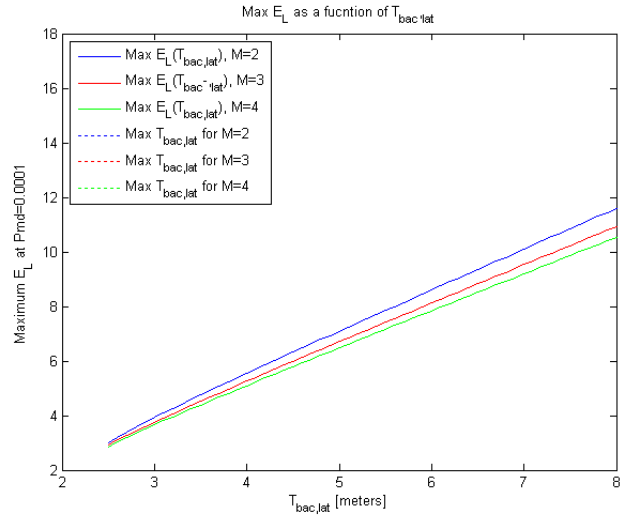

Figure 22 Maximum E_L as a Function of the Lateral RRFM Threshold

REFERENCES

1 ICAO NSP May 2010 WP 59, "Development Baseline SARPs Proposal", presented by Tim Murphy, Montreal, 17-28 May 2010.

2 ICAO NSP Nov 09 WGW/Flimsy 6, "Conceptual Framework for the Proposal for GBAS to Support CAT III Operations".

3 Clark, B., & B. DeCleene, "Alert Limits: Do We Need Them for CAT III?", Proceedings of ION GNSS 2006, Fort Worth, TX, 26 – 29 September 2006.

4 Shively, C., "Comparison of Methods for Deriving Ground Monitor Requirements for CAT IIIB LAAS", Proceedings of ION National Technical Meeting, San Diego, CA, 22 – 49 Jan 2007.

5 ICAO NSP WG 1&2 IP 18, "Vertical Alert Limit Requirement for a Level of Service of GBAS Appropriate to Support CAT II/III Operations", Bruce DeCleene, Montreal Oct 2005.

6 Murphy, T. "Development of Signal in Space Performance Requirements for GBAS to Support CAT II/III Landing Operations", Proceedings of the ION GPS 2001.

7 Murphy, T. "Considerations for GBAS Service Levels to Support CAT II/III Precision Approach", ICAO GNSSP-WP-19 Meeting, Yokohama, Oct 2000.

8 FAA Advisory Circular 120-28D, "Criteria for Approval of Category III Weather Minima for Takeoff, Landing and Rollout" dated July 13, 1999.

9 EASA, CS AWO 1, "Joint Aviation Requirements – All Weather Operations", Subpart 1, "Automatic Landing Systems".

10 Miller, D., et. al. "Development of Local Area Augmentation System Requirements", Proceedings of ION GPS-96, Sept 1996.

11 ICAO NSP May 10 WGW/WP 19, "SARPS Support for Airworthiness Assessments -More on GLS Signal Modeling", presented by Tim Murphy, Montreal, 17-28 May 2010.

12 ICAO NSP Mar 09 WGW/WP 30 "SARPS Support for Airworthiness Assessments GLS Signal Modeling", presented by Tim Murphy, Bretigny, 17-27 March 2009.

13 P.Neri, C.Macabiau, L.Azoulai, "Proceedings of the IEEE Position Location and Navigation Systems (PLANS) Conference, May 2010, San Diego.

14 ICAO NSP Nov 09 WGW/IP 9, "GAST D GBAS Signal Model Assessment by ENAC and AIRBUS", Presented by Tim Murphy, November 2009.

15 P.Neri, C.Macabiau, L.Azoulai, "Study of a GBAS Model for Cat II/III Simulations", ION GNSS 2009, Savannah (GA, US).

16 Boeing Document D6-83447-5, "Volume V – Characterization of the GBAS System Output", Rev New, Dated October 19, 2005.

17 ICAO NSP WGW IP/17, "A Noise Model for Simulation of Nominal GBAS Errors to Support Airworthiness Certifications", Navigation Systems Panel, CAT II/III Subgroup (CSG), Montreal, 18-20 Oct 2004.

18 Juan-Jose Navarro, "GBAS Position Error Model", EUROCAE WG 28, Working Paper 11/ March 2002, Germany.

19 Murphy, T; Anderson, L.; Harris, Matt; Tang, N. "CAT III Simulated Landing Performance for ILS and GLS", Proceedings of the ION GPS 2001, Sept 2001, Salt Lake City.

20 Nam, Y et. al. "A GBAS Landing System Model for CAT I", Proceedings of the International Association of Institutes of Navigation (IAIN) conference, June 2000, San Diego.

21 Young Nam and Tom Zalesak, "GPS/LAAS Certification Model", internal NAWCAD Report (not generally available but largely reproduced in reference [22]).

22 ICAO Paper GNSSP-WP-8, Validation of GBAS CAT I Accuracy: A GLS Model and Autoland Simulations for Boeing Airplanes, presented at the ICAO Global Navigation Satellite Systems Panel, Working Group B Meeting, Seattle, WA, May 29 - June 9, 2000.

23 McGraw, G. et. al. "Development of the LAAS Accuracy Models", Proceedings of ION GPS-2000, Sept 2000.

24 Braasch, M. McGraw, G, "GPS Receiver Tracking Loop Modeling to Support Autoland Simulations", Proceedings of the ION National Technical Meeting 1996.

25 Ravier, C. Rambach, D. Plantecoste, MO. Azoulai, L, "GBAS Cat 2/3 Failures Assessment", presented to RTCA SC 159 WG 4 and AWO HWG, October 2009.

26 EASA CS 25.1309, Large Aeroplanes - Equipment, Systems and Installation.

27 FAA Advisory Circular 25.1309-1A "System Design and Analysis", dated 6/21/88.

28 EASA AMC 25.1329 Automatic pilot.

29 FAA Advisory Circular 25.1329-1B "Approval of Flight Guidance Systems", dated 7/17/06.

30 Ravier, C. Azoulai, L. Rambach, D, "Vertical Criterion for GAST D Failures Assessment", presented to RTCA SC 159 WG 2C and WG 4, June 2010.

31 Brenner, M. et. al. "RTCA SC-159 WG2 Position Paper (version 1)", presented to RTCA SC 159 WG 2C, Jan 2009.

32 Annex 10 to the Convention on International Civil Aviation, Volume 1, "Radio Navigation Aids", Attachment G Section 2.5.2 and Figure G-1.

33 ICAO NSP May 2010 WGW/WP 16, "Computation of Maximum Undetected Error for RRFM in Support of Airworthiness Assessments", Navigation Systems Panel, Working Group of the Whole, Montreal, 17-28 May 2010.

34 ICAO NSP May 2010 WGW/WP 14, "Validation of Ionospheric Anomaly Mitigation for GAST D", Navigation Systems Panel, Working Group of the Whole, Montreal, 17-28 May 2010.

35 ICAO NSP Nov 2009 WGW/WP 28, "Validation of GAST D Mitigation of Errors Induced by Ionospheric Decorrelation ", Montreal, November 2009..

36 RTCA DO-253C, "Minimum Operational Performance Standards for GPS Local Area Augmentation System Airborne Equipment", dated Dec 16th 2008.

37 ICAO NSP July 09 CSG/WP 10, "GAST D Single Ground Subsystem Reference Receiver Fault Requirements Report of the H1 Ad-hoc Group".

38 Luo, M., et. al., "Ionosphere Spatial Gradient Threat for LAAS: Mitigation and Tolerable Threat Space", Proceedings of the ION National Technical Meeting, Jan. 2004.

39 Luo, M. et. al., "LAAS Study of Slow-Moving Ionosphere Anomalies and Their Potential Impacts", Proceedings of the Institute of Navigation, GNSS Conference, Sept. 2005.

40 S. Pullen, Y.S. Park, and P. Enge, "Impact and Mitigation of Ionospheric Anomalies on Ground-based Augmentation of GNSS," Radio Science, Vol. 44, Aug. 2009.

41 S. Datta-Barua, J. Lee, et al, "Ionospheric Threat Parameterization for Local Area GPS-Based Aircraft Landing Systems," Submitted to AIAA Journal of Guidance, Control, and Dynamics, Aug. 2009.

42 S. Ramakrishnan, J. Lee, S. Pullen, and P. Enge, "Targeted Ephemeris Decorrelation Parameter Inflation for Improved LAAS Availability During Severe Ionosphere Anomalies," Proceedings of the ION 2008 National Technical Meeting, San Diego, CA, USA, Jan. 28-30, 2008.

43 ICAO NSP/WG1 WP 26, "Mitigation of Iono Gradient Threat for GSL D", New Delhi, March 6th 2007.

44 Susumu Saito, Takayuki Yoshihara, and Naoki Fujii, "Development of an Ionospheric Delay Model with Plasma Bubbles for GBAS", Electronic Navigation Research Institute, Japan – Appendix 1 to IP 4 - NSP March 09 WGW/IP4,Brétigny-sur-Orge, 17 – 27 March 2009.

45 Murphy, T., Harris, M., "Mitigation of Ionospheric Gradient Threats for GBAS to Support CAT II/III", Proceedings of the ION GNSS 2006.

46 Murphy, T., Harris, M., "More Ionosphere Anomaly Mitigation Considerations for Category II/III GBAS", Proceedings of the ION GNSS 2007.

47 CSG July 2009 WP 17, "Ionosphere Anomaly Monitors Validation Status 09071", Presented by Tim Murphy, July 2009, Seattle.

48 ICAO NSP/WGW Flimsy 7 "GAST D SARPS Proposal Current Baseline", presented by Tim Murphy, Montreal, November 2009.

49 ICAO NSP WGW/WP 29, "Standard Threat Model Used in GAST D Ionospheric Monitoring Validation "Presented by Tim Murphy, November 2009.

50 ICAO NSP May 2010 WGW/WP 14, "Validation of Ionospheric Anomaly Mitigation for GAST D", Navigation Systems Panel, Working Group of the Whole, Montreal, 17-28 May 2010.

51 ICAO NSP WGW/WP 28, "Validation of GAST D Mitigation of Errors Induced by Ionospheric Decorrelation ", Montreal, November 2009.

52 ICAO NSP May10 WGW/WP19, "Computation of Maximum Undetected Error for RRFM in Support of Airworthiness Assessments".

53 Shively, C. “Derivation of Vertical Alert Limit for LAAS CAT III Autoland Considering Limit Risk Requirement”, Institute of Navigation Annual Meeting 2004.

54 Shively , C. "GBAS GAST-D Aircraft Monitor Performance Requirements for Single Reference Receiver Faults", ION NTM 2009.